

Broadband Ultrasound Field Mapping System Using a Wavelength Tuned, Optically Scanned Focused Laser Beam to Address a Fabry Perot Polymer Film Sensor

Edward Zhang and Paul Beard

Abstract—An optical system for rapidly mapping broadband ultrasound fields with high spatial resolution has been developed. The transduction mechanism is based upon the detection of acoustically induced changes in the optical thickness of a thin polymer film acting as a Fabry Perot sensing interferometer (FPI). By using a PC-controlled galvanometer mirror to line-scan a focused laser beam over the surface of the FPI, and a wavelength-tuned phase bias control system to optimally set the FPI working point, a notional 1D ultrasound array was synthesized. This system enabled ultrasound fields to be mapped over an aperture of 40 mm, in 50- μm steps with an optically defined element size of 50 μm and an acquisition time of 50 ms per step. The sensor comprised a 38- μm polymer film FPI which was directly vacuum-deposited onto an impedance-matched polycarbonate backing stub. The -3 dB acoustic bandwidth of the sensor was 300 kHz to 28 MHz and the peak noise-equivalent-pressure was 10 kPa over a 20-MHz measurement bandwidth. To demonstrate the system, the outputs of various planar and focused pulsed ultrasound transducers with operating frequencies in the range 3.5 to 20 MHz were mapped. It is considered that this approach offers a practical and inexpensive alternative to piezoelectric-based arrays and scanning systems for rapid transducer field characterization and biomedical and industrial ultrasonic imaging applications.

I. INTRODUCTION

MAPPING broadband ultrasound fields in water, for characterization or imaging purposes, is most commonly achieved using piezoelectric detectors, either by mechanically scanning a single element or by using an array of elements. Limitations associated with piezoelectric detectors include the difficulty in achieving the necessary acoustically small element sizes ($< 100 \mu\text{m}$) at megahertz frequencies to avoid spatial averaging while retaining adequate detection sensitivity. Additionally, in the case of systems based upon the use of a mechanically scanned element, acquisition speed can be unacceptably low and the use of an array of detectors to overcome this can be prohibitively expensive on account of the high channel counts required to spatially sample with adequate resolution over usefully large acoustic apertures.

Manuscript received September 12, 2005; accepted February 16, 2006. This work was supported by the UK EPSRC.

The authors are with the Department of Medical Physics and Bioengineering, University College London, London, WC1E 6BT, UK (e-mail: e.zhang@medphys.ucl.ac.uk).

There is the potential to overcome these limitations using optical ultrasound mapping techniques. This is particularly so where the mapping is achieved by optically addressing the output of a continuously sensitive optical sensor (as opposed to the use of an array of discrete sensors or a mechanically scanned single element). This can be achieved either in a sequential fashion by rapidly scanning a single focused laser beam over the sensor, or in parallel by illuminating with a large area beam and spatially resolving the sensor output with an array of photodetectors. Either way, by encoding the spatial distribution of the acoustic field onto an optical field, there is the prospect of obtaining effective element sizes and spatial sampling intervals significantly smaller than can be achieved with piezoelectric receivers, in principle down to the optical diffraction limit of a few microns. Furthermore, high speed mapping can be inexpensively achieved using galvanometer or electro-optic scanners, if the sensor output is being addressed sequentially, or using an array of photodetectors such as a charge-coupled device (CCD), if in parallel.

Several field mapping approaches of this nature, based upon a variety of transduction mechanisms, have been investigated. Among these are the use of a CCD array to map acoustically induced changes in the optical reflectance at a glass-liquid interface [1]. The use of a scanned focused laser beam to directly detect acoustic displacements using remote Fabry Perot [2] and Mach Zender [3] receiving interferometers has also been explored. Another category of interferometric techniques is based upon the detection of acoustically induced changes in the optical thickness of multilayer dielectric stack [4]–[6], glass [7] and polymer film [8]–[10] Fabry Perot (FP) sensing interferometers. The broadband high sensitivity of the last of these, comparable to piezoelectric polyvinylidene fluoride (PVDF) detectors, is particularly promising and has now been demonstrated in a variety of configurations for field mapping. One approach has been to employ a large area laser beam to illuminate the sensor, an angle-tuned scheme to set the phase bias, and a mechanically scanned photodiode to detect the sensor output in order to synthesize a two-dimensional (2D) ultrasound receive array [11], [12]. Another approach employed a similar scheme with the exception that a 2D CCD array was used to map the sensor output in parallel rather than sequentially [13]. In the current paper, we provide details of an alternative method in which the sensor is

optically addressed using a single focused laser beam that is scanned across the sensor and the phase bias control achieved by wavelength tuning. This offers the prospect of scanning over much larger apertures than have been previously obtained, along with significantly smaller optically defined element sizes. Furthermore, it makes optimal use of the available laser power to provide high sensitivity and, through the use of a high-speed galvanometer scanning system, much faster acquisition rates. The underlying feasibility of the concept was first reported in a preliminary account [14]. In this paper we provide a detailed description of the operating principles of the instrument, its performance, and specific application to transducer field characterization.

Section II describes the design and fabrication of the sensor head and the optical scanning system used to interrogate and map its output. Section III describes the performance of the system in terms of its spatial scanning parameters and the acoustic performance of the sensor. In Section IV, the practical application of the system to mapping the output of a variety of broadband transducers is demonstrated.

II. FP ULTRASOUND LINE-SCANNING SYSTEM

The underlying principle is one in which a Fabry Perot polymer film sensing interferometer (FPI) is illuminated with a focused laser beam that is rapidly line-scanned step by step over the sensor using a high-speed precision galvanometer mirror. At each point of the scan, the sensor is optimally biased by tuning the laser wavelength to the point of maximum slope on the FP interferometer transfer function (ITF), the relationship between reflected optical power and phase. An incident ultrasound wave modulates the optical thickness of the polymer film FPI, producing a small optical phase shift. This is linearly converted, via the ITF, to a corresponding reflected intensity modulation which is detected by a photodiode. By recording the temporal output of the photodiode using a high-speed digitizer at each point of the scan, the lateral and temporal distribution of the incident acoustic field can therefore be mapped. In this way, the system can be regarded as a notional linear ultrasound array, the aperture of which is defined by the length of the line-scan and the element size and the interelement spacing by the spot size of the laser beam and the scan increment, respectively. The experimental realization of this approach comprises three essential components: (1) the FP sensor head (Section II-A), (2) the optical system used to illuminate the sensor and map its output (Section II-B), and (3) the wavelength-tuned phase bias control scheme for setting working point of the FPI (Section II-C).

A. FP Sensor Head

The design and fabrication of the FP sensor is similar to that described in [12]. Briefly, the sensor comprises an opti-

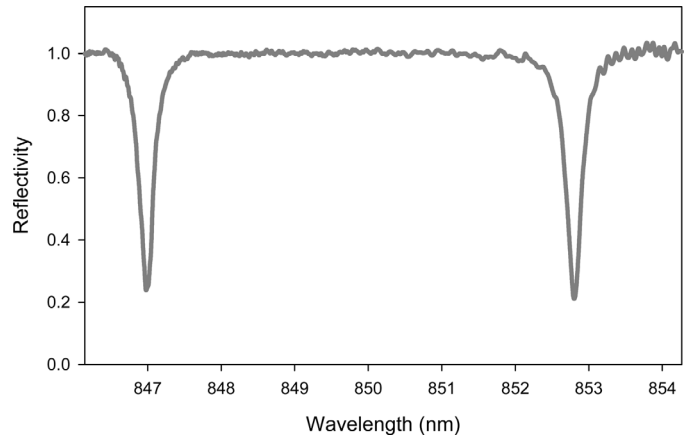


Fig. 1. Measured reflectivity wavelength transfer function of the FP sensor.

cally transparent polycarbonate backing stub of thickness 11.5 mm and lateral dimensions 50×30 mm onto which a multilayer structure that formed a polymer film FPI was vacuum deposited. The first mirror of the FPI was formed by depositing a multilayer soft dielectric coating with a nominal reflectivity of 92% at 850 nm directly onto the backing stub. This was followed by the vacuum deposition of a 38- μm -thick Parylene C polymer film spacer of refractive index 1.65. A fully opaque gold coating (with a chrome layer precursor to aid adhesion) of estimated reflectivity 80% was deposited on top of the Parylene spacer to form the second FPI mirror. Finally, a 4- μm -thick Parylene C barrier coating was deposited over the entire structure to protect the external reflective gold coating from damage due to abrasion or water ingress.

The fabrication procedure outlined above has a number of advantages. These are principally derived from the ability to vacuum deposit the Parylene film spacer directly from the gas phase [12]. The excellent uniformity of optical thickness ($< \lambda/4$ over 1 cm at 850 nm) and surface finish that this process affords enables a high quality FPI with good visibility and finesse to be produced. The thickness can also be precisely controlled ($< 0.1 \mu\text{m}$) to design sensors with specific free spectral ranges and acoustic bandwidths. Additionally, the sensor can be inexpensively batch fabricated in large quantities with high repeatability. Finally, previous experience has shown that sensors fabricated using this process are extremely rugged, rarely failing despite long periods of immersion in water, and provide many years of reliable operation.

The measured reflectivity wavelength transfer function of the sensor is shown in Fig. 1. This was obtained by illuminating the sensor with a 50- μm -diameter laser beam at normal incidence, varying the laser wavelength over 7.8 nm and measuring the reflected power from the sensor as a proportion of the incident power. From the transfer function shown in Fig. 1, the measured reflectivity finesse is $F_R = 26$, the fringe visibility $V = 0.6$, and the free spectral range $FSR = 5.83$ nm.

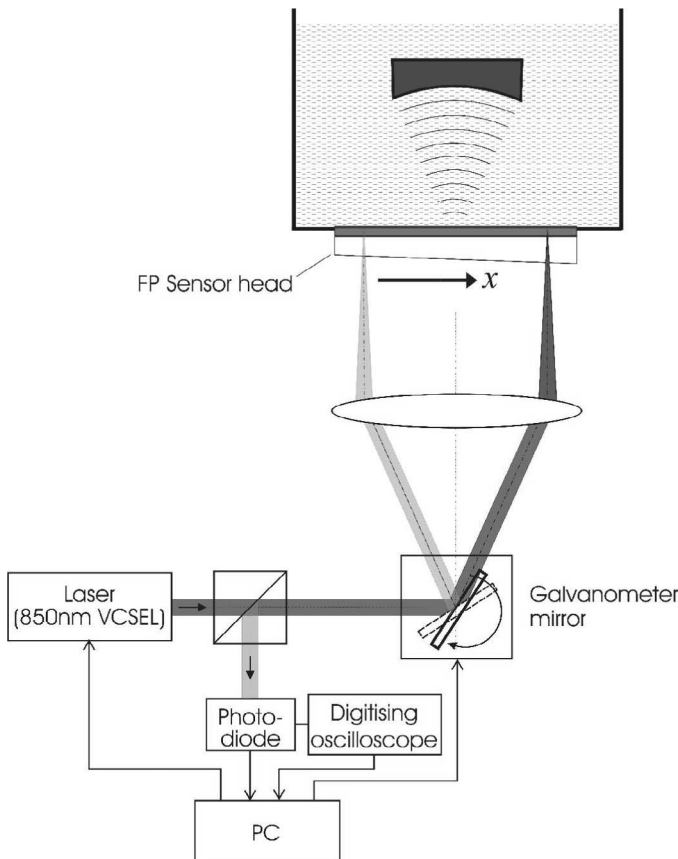


Fig. 2. Schematic of line-scanning ultrasound field mapping system.

B. Optical Scanning System

An optical system based on a moving coil galvanometer was used to scan a focused interrogating laser beam across the surface of the FP sensor (Fig. 2). The laser source is an uncooled 0.5-mW 850-nm vertical cavity surface emitting laser (VCSEL) operating in single longitudinal mode. The injection current to the VCSEL is provided by a laser diode driver operating in constant current mode that is controlled via a 12-bit D-A card within the PC. The collimated output beam of the VCSEL is incident on the rotation axis of a high-speed precision galvanometer mirror (GSI Lumonics, Ltd., Rugby, UK), the angle of rotation of which is also controlled via the PC D-A card. The galvanometer mirror is positioned at the focus of a lens, an achromatic doublet, of diameter 50 mm and focal length 75 mm, and above this, in the focal plane of the lens, the FP sensor is situated. This arrangement enables a normally incident focused laser beam of 50 μm diameter to be line-scanned over a length of 40 mm in steps of 10 μm . The beam reflected from the sensor is directed via a beamsplitter onto a 30-MHz dc-coupled silicon photodiode/transimpedance amplifier configuration. The voltage output of the photodiode is high pass (> 300 kHz) filtered to remove the dc optical component reflected from the sensor and the low frequency intensity fluctuations produced by the VCSEL and is measured using a digitizing oscilloscope (DSO) connected to the PC via a general purpose in-

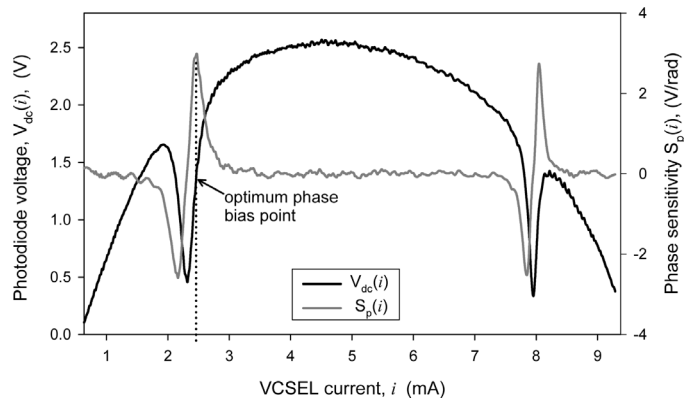


Fig. 3. Output of wavelength tuned phase bias control scheme showing the reflected output $V_{dc}(i)$ and the corresponding phase sensitivity $S_p(i)$ as a function of the VCSEL injection current i . The vertical dotted line indicates the current at which the phase sensitivity is a maximum, the optimum operating point of the sensor.

terface board (GPIB) interface. The DSO is used to record the small time-varying reflected intensity output of the sensor produced by an incident acoustic wave. The photodiode output is also connected to a low-speed (10 KHz) dc-coupled A-D card within the PC. The resulting digitized signal is referred to as the low-pass filtered photodiode output. This is used to record the reflected power output of the FPI as the VCSEL wavelength is tuned as part of the procedure to set the optimum phase bias point of the sensor, as described in the next section.

C. Phase Bias Control Scheme

In principle, to map an acoustic field, the focused laser beam can be scanned over the FP sensor surface and the acoustic signal captured by the DSO at each point of the scan. However, the sensitivity of the FP sensor varies from point to point as a result of changes in the slope of the ITF (the relationship between reflected power and optical phase) due to variations in the optical thickness of the polymer film. To overcome this and interrogate any point on the FPI with optimum sensitivity, the wavelength of the VCSEL is electronically tuned by varying its injection current so as to optimally set the phase bias of the FPI at each point of the line-scan. This is achieved by tuning the laser wavelength over the free spectral range (FSR) of the FPI in order to recover the ITF and then returning to the wavelength that corresponds to the peak value of the ITF phase derivative, the point of maximum sensitivity.

The practical implementation of this requires the following steps. First, a linear current ramp generated by the PC is applied to the VCSEL. The corresponding reflected intensity output of the FP sensor is monitored by recording the low-pass filtered output of the photodiode $V_{dc}(i)$ as a function of the VCSEL current i . An example of this is provided in Fig. 3. The two sharp reflectance minima of the FPI due to the change in VCSEL wavelength with current $d\lambda(i)$ are superimposed on the relatively gradual rise and subsequent fall of the VCSEL output power with

current; the latter is represented by $\overline{P}_{vo}(i)$, a scaling factor normalized to the maximum power output of the VCSEL. Note that $V_{dc}(i)$ itself is not a direct representation of the ITF due to the nonlinear nature of both $\overline{P}_{vo}(i)$ and $d\lambda(i)$ —the latter being evidenced by the reduced width of the second FPI minima due to the increased rate of wavelength change at higher currents. To obtain the ITF from $V_{dc}(i)$, the VCSEL output characteristics need to be accounted for by taking the following steps. First, the ratio $\overline{V}_{dc}(i) = V_{dc}(i)/\overline{P}_{vo}(i)$ is calculated to remove the effect of the variation of the VCSEL output power with current and thus provide a measure of the wavelength dependent reflectivity of the sensor. Second, the phase shift $\phi(i)$ due to the current-induced wavelength change $d\lambda(i)$ is obtained using the expression $\phi(i) = 4\pi n l d\lambda(i)/\lambda^2$, where l and n are the thickness and refractive index, respectively, of the Parylene polymer film and λ is the center wavelength (850 nm) of the VCSEL. The reflected sensor output can now be expressed as a function of phase shift, $\overline{V}_{dc}(\phi(i))$, which provides a direct representation of the ITF. The phase derivative of this is then calculated and, in a final step, multiplied by $\overline{P}_{vo}(i)$ to incorporate the VCSEL output power characteristics. This yields the relative phase sensitivity $S_p(i)$, a measure of the sensitivity of the FPI to an acoustically induced phase shift [15], for each value of the VCSEL current, thus

$$S_p(i) = [d\overline{V}_{dc}(\phi(i))/d\phi(i)]\overline{P}_{vo}(i). \quad (1)$$

The sensor can now be optimally biased by setting the VCSEL current to that corresponding to the maximum value of $S_p(i)$, as shown in Fig. 3. In this example, this occurs at the peak positive slope of the first fringe due to the higher output power of the laser at this current compared to that corresponding to the second fringe.

An essential requirement for the successful implementation of this approach is accurate knowledge of the VCSEL output power and wavelength characteristics, $\overline{P}_{vo}(i)$ and $d\lambda(i)$, respectively, since neither vary linearly with current. To obtain $\overline{P}_{vo}(i)$, the FP sensor was replaced with a broadband mirror and the photodiode output recorded as a function of i . $d\lambda(i)$ was obtained by calibrating the system against a 1.5-mm-thick low finesse reference etalon. The latter was positioned in place of the FP sensor, a linear current ramp applied to the VCSEL, and the corresponding sinusoidally varying reflected intensity from the etalon recorded. By noting the values of i corresponding to successive peaks and troughs in the etalon output, each of which represent a phase excursion of π radians, and assuming a linear relationship between wavelength change and phase shift over the small wavelength range (< 10 nm) involved, $d\lambda(i)$ was determined.

It is noted that the use of a VCSEL as the interrogating laser source offers a number of advantages. First, it has a high electronic-wavelength tuning coefficient, at least 0.6 nm/mA, which is approximately an order of magnitude higher than that of a conventional 850-nm edge-emitting semiconductor laser diode (typically < 0.02 nm/mA). This enabled continuous tuning ranges of up to 9.5 nm to be

obtained, sufficient to tune over the FSR of sensors with thicknesses down to 22 μm . Second, it offers millisecond tuning times, making it possible to recover the ITF and locate the optimum phase bias “on the fly” as the laser spot is being scanned across the surface of the sensor for high-speed mapping. Finally, at a cost of less than \$50, the VCSEL is an inexpensive alternative to external cavity lasers and other continuously widely tunable lasers used for interrogating this type of sensor.

D. Waveform Acquisition and Processing

To map the output of the sensor, the focused laser beam is scanned step by step along a line over the FP sensor. At each step of the scan, the optimum phase bias point is first set by adjusting the laser wavelength under PC control, as described in Section II-C, and the detected acoustic waveform is then captured using the DSO. Two approaches to transferring the waveforms from the DSO to the PC were investigated. The first involves capturing a waveform at each point of the scan and immediately downloading it to the PC via the GPIB interface before moving on to the next point. This method was used for the line-scans of the planar transducers shown in Section IV-A. However, the relatively slow access time of the GPIB interface resulted in a significant delay of approximately 1 s per scan step. To avoid this, an alternative approach using the “Fastframe” segmented memory feature of a Tektronix TDS784D (Tektronix, Bracknell, UK) DSO was investigated and used for the measurement of the focused transducer described in Section IV-B. This method allows successive acoustic waveforms, one for each step of the line-scan, to be captured on a single continuous record on the DSO. This is implemented in practice by generating an “enable” signal once the laser beam has moved one step and the phase bias control procedure completed. The enable signal is then used to prepare the DSO to make a triggered acquisition, the actual triggering of which occurs on receipt of the synchronization signal provided by the source used to generate the ultrasound signal. Once the acquisition has been triggered, the enable signal is reset so that the DSO is disabled. No further acquisitions can then be made until the system has advanced to the next point in the scan, ensuring that only a single acquisition at each scan point is made. The “Fastframe” or segmented memory feature of the DSO stores each acquisition in its own numbered memory segment and concatenates all of the segments to form a single long record containing all of the waveforms. This record, which is stored within the on-board memory of the DSO, is then downloaded to the PC in a single step at the end of the scan, eliminating the time penalties in transferring the waveforms to the PC at each point of the scan. The point-to-point acquisition time is therefore limited only by the galvanometer response time, the wavelength tuning speed of the VCSEL, and the associated control electronics.

In addition to the acoustic waveform being recorded, the value of the relative phase sensitivity $S_p(i)$ is recorded at

each point of the scan. By dividing the captured waveform by $S_p(i)$, variations in phase sensitivity across the sensor can be compensated for. These are principally as a result of variations in the VCSEL output power due to the different currents required to optimally bias the sensor at different points on the sensor and, to a lesser extent, variations in the FPI mirror reflectivities or defects in the Parylene film spacer.

III. SYSTEM PERFORMANCE

The following subsections describe the performance of the system in terms of the essential parameters required to specify an ultrasound field mapping system: namely, the extent and spatial sampling parameters of the acoustic aperture, acquisition speed, and the acoustic performance in terms of sensitivity, linearity, and frequency response.

A. Scan Parameters: Line-Scan Length, Spatial Sampling Interval, and Spot Size

The system shown in Fig. 2 is capable of scanning a focused spot of 50- μm -diameter over a line of length 40 mm in steps of 10 μm ; these parameters were verified by scanning a spatially calibrated imaging target composed of parallel reflective chrome lines deposited onto a glass substrate. There is further scope to optimize the system for specific applications. For example, the spot size could be reduced further, in principle down to the optical diffraction limit of a few microns for high frequency applications, either by increasing the beam diameter of the collimated output of the VCSEL or by reducing the focal length of the lens. There is inevitably a compromise with either option. For example, if the focal length is reduced, the galvanometer would have to be placed closer to the lens, thus reducing the length of the line-scan due to the limited angular range (40°) of the galvanometer. In addition, the increased off-axis aberration exhibited by a lens of shorter focal length will, for large angular excursions, distort the geometry of the spot and alter the step interval. As a consequence, this will reduce the dimensions over which the acoustic aperture can be accurately sampled. Conversely, for applications where an increased spot size can be tolerated, an increased line-scan length can be obtained by using a lens of longer focal length. The minimum scan step size is ultimately limited by the 0.00058° angular resolution of the galvanometer to 0.076 μm (for the lens used in this study), although in this study the 12-bit resolution of the PC D-A card limited the step size to approximately 10 μm .

B. Acquisition Speed

Given the rapid response of the galvanometer (its small angle step response time is less than 0.5 ms), and the ability to store successive acoustic waveforms acquired over a

line-scan on a single record on the DSO (described in Section II-D) which eliminates the time penalties involved in the downloading to the PC at each scan step, the minimum achievable acquisition time is limited primarily by the tuning speed of the VCSEL. Although this can be as rapid as a few tens of microseconds when scanning the wavelength over the FSR of the FPI, a relatively long settling period is required to establish the necessary thermal equilibrium for a stable output once the system has located the optimum sensor operating current. This ultimately limits the minimum time period required to complete the phase bias control procedure described in Section II-C to a few milliseconds. In this study, the tuning speed was further limited by the D-A card used to control the VCSEL. For this reason, the minimum time taken to scan from one point to the next, set the FPI optimum phase bias, and capture the acoustic waveform was 50 ms.

C. Acoustic Performance

1. *Detection Sensitivity:* The detection sensitivity or noise-equivalent pressure (NEP) is defined as the acoustic pressure that provides a system signal-to-noise ratio of unity in the low frequency limit [15] $\lambda_a \gg l$ where λ_a is the acoustic wavelength and l the FPI thickness. The NEP therefore represents the minimum detectable acoustic pressure and is given by

$$\text{NEP} = \frac{N}{S}, \quad (2)$$

where S is the sensor sensitivity and is defined as the reflected optical power modulation per unit acoustic pressure ($\mu\text{W}/\text{MPa}$) at the FPI optimum phase bias point [15]. S is proportional to the phase sensitivity and therefore depends on the shape of the ITF which, in turn, is a function of various fixed parameters such as the reflectivities and absorbance of the FPI mirrors and the phase dispersion imposed by the geometry of the laser beam and nonuniformities in the polymer film spacer. S also depends on the thickness and elastic and photoelastic properties of the polymer film and the acoustic impedance of the backing stub [15]. N is the minimum detectable optical power modulation reflected from the sensor over a specified measurement bandwidth and is a function of the noise characteristics of the laser source and the photodiode/transimpedance amplifier configuration. In contrast to previous FP sensor systems [12], [16], the noise characteristics of the former dominates in this system due to the relatively low side-mode suppression ratio of the VCSEL.

S , and to a lesser extent N , also depend upon the incident optical power. This varies across the line-scan as the operating current of the VCSEL required to optimally bias the sensor is also position dependent. Although the variations in S due to this (and other factors) are corrected for by normalizing to the measured relative phase sensitivity $S_p(i)$ at each point of the scan, as described in Section II-D, this procedure also results in the nominally constant N being scaled by $S_p(i)$. Thus N , and therefore the NEP,

will, to some degree, be position dependent. However, it is still possible to quote a meaningful approximate figure for the NEP as the optimum operating currents along a specific line-scan tend to be clustered over a relatively small current range. By measuring the sensor output in response to the output of a calibrated lead-zirconate-titanate (PZT) ultrasound source operating at a nominal center frequency of 3.5 MHz, the NEP was found to be 10 kPa over a 20-MHz measurement bandwidth without signal averaging. This corresponds to a noise-equivalent-phase shift of 0.6 mrad. Note that these noise equivalent figures are peak values, not rms, as it is considered the former provides a more realistic indication of the smallest signal that can be detected when measuring broadband signals in the time domain.

2. Linearity: Assuming the elastic limits of the polymer film and the linear operating range of the photodiode are not exceeded, the upper limit of linear acoustic detection is determined by the phase range over which the ITF is linear and the acoustic phase sensitivity, the magnitude of the optical phase shift produced per unit acoustic pressure [15]. For the sensor used, the linear phase range around the optimum phase bias point is 0.072 rad. This was obtained by using an Airy Function to compute an ITF for an FPI of the same reflectivity finesse ($F_r = 26$) as the sensor and then determining the phase excursion over which the ITF departed from a linear relationship by 10%. Using a value for the acoustic phase sensitivity of 0.06 rad/MPa (based on a previously reported value of 0.15 rad/MPa for a 50- μm -thick rigid-backed Parylene film [17]), this corresponds to an upper limit of linear detection of 1.2 MPa.

3. Frequency Response: Assuming the sensor operates predominantly in the thickness mode, the bandwidth for a normally incident plane wave is determined by the thickness and speed of sound of the polymer film and the acoustic impedance of the backing material. The uniformity of response is determined by the acoustic impedance mismatches at the boundaries of the film, on one side due to the backing, on the other due to the surrounding water [15]. In general, polymer films have an acoustic impedance close to water, and uniform broadband response characteristics can therefore be expected. This can be seen in Fig. 4, which shows the predicted normalized acoustic phase sensitivity [15] (the acoustically induced phase shift per unit pressure) as a function of frequency for a normally incident plane wave. This was obtained using an experimentally validated analytic model that calculates the frequency-dependent mean distribution of stress across the polymer film thickness by the summation of acoustic reflections within the film. The model is essentially as described in [15] with a modification to incorporate the effect of the barrier coating.

The close acoustic impedance match between the Parylene film ($Z_{ppxc} = 2.88 \times 10^6 \text{ Kg/m}^2\text{s}$) and the polycarbonate ($Z_{pc} = 2.7 \times 10^6 \text{ Kg/m}^2\text{s}$) backing means that the response falls off smoothly without resonances to a min-

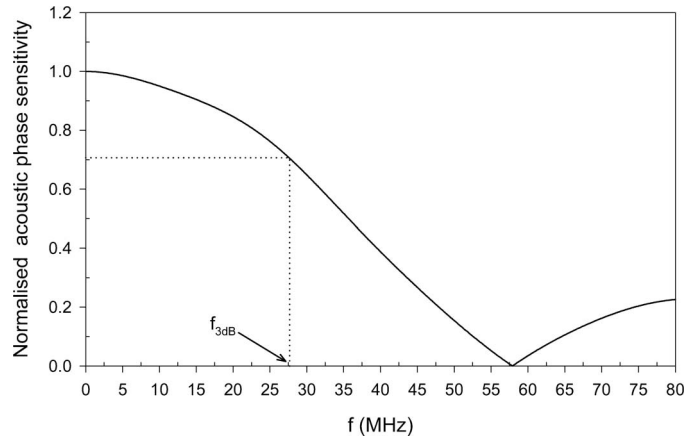


Fig. 4. Predicted normalized sensor frequency response characteristics.

imum at 57.9 MHz when $\lambda_a = l$ with a -3 dB bandwidth of 27.8 MHz. The small difference between Z_{pc} and Z_{ppxc} does have a noticeable influence on the frequency response—the curve in Fig. 4 does not quite display the damped co-sinusoidal shape characteristic of a perfectly matched configuration. Nevertheless, the broader band, more uniform frequency response characteristics obtained using a polymer, rather than a glass backing as with previous sensors [12], [15], is evident.

There are two factors to be noted in relation to the low frequency response of the sensor. First, acoustic reflections within the polycarbonate backing stub due to its finite thickness (which the model assumes is of infinite extent) could, in principle, perturb the frequency response. This would occur at relatively low frequencies, comparable to the reciprocal of the acoustic round trip transit time through the stub: around 100 kHz for the 11.5-mm-thick polycarbonate stub for the sensor used in this study. However, the amplitude of these reflections, and hence their influence on the frequency response characteristics, is strongly reduced by the high acoustic attenuation (typically $> 25 \text{ dB}$ at 3.5 MHz) incurred in traveling through 23 mm of polycarbonate. This suggests that, although this sensor has been primarily developed for measuring pulsed fields centered at megahertz frequencies, its design would not necessarily preclude its application to the measurement of low frequency continuous wave (CW), quasi CW, or long pulse transient fields. Second, Fig. 4 represents the intrinsic frequency response of the FP sensor and thus does not include the low frequency roll-off due to the 300-KHz high-pass filter referred to in Section II-B.

IV. SYSTEM EVALUATION

To demonstrate the system, the outputs of a variety of planar and focused pulsed PZT ultrasound transducers with center frequencies in the range 3.5 to 20 MHz were mapped. The transducers were driven by an electrical pulse generator (Panametrics Model 500PR) which provided a single negative pulse at a repetition frequency of 6 kHz.

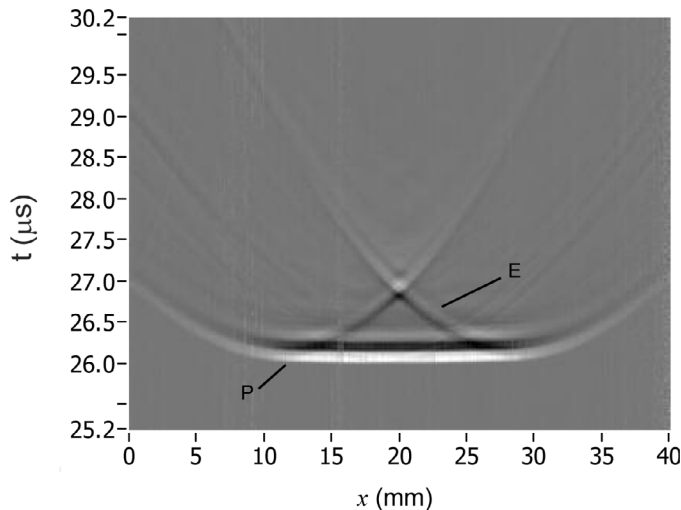


Fig. 5. Line-scan of the output of a pulsed 3.5-MHz planar PZT transducer of diameter 22 mm positioned 38 mm from the FP sensor. P: initial plane wave, E: edge wave component. Line-scan length $x = 40$ mm, scan step $dx = 50 \mu\text{m}$, spot size $a = 50 \mu\text{m}$, temporal sampling interval $dt = 4$ ns, number of signal averages = 128, image acquisition time = 13.5 minutes.

A. Line-Scans of Planar Transducers

In the first instance, the output of a relatively large-diameter (22 mm) 3.5-MHz PZT planar transducer (Panametrics V381, Olympus NDT U.K., Ltd., Rotherham, South Yorkshire, UK) was scanned in order to demonstrate the ability of the system to map signals over its maximum line-scan length of 40 mm. The transducer was aligned parallel to the detection plane at a distance of 38 mm from the sensor in a water bath. The peak positive acoustic pressure output of the transducer was approximately 0.05 MPa. The interrogation laser beam was scanned in steps of $50 \mu\text{m}$ along a line of length 40 mm in the x direction that passed through the transducer axis. At each point of the scan, a portion of the time record of the high-pass filtered photodiode output, which represents the acoustic waveform, was signal averaged over 128 pulses and captured by the DSO, using a delayed trigger, and downloaded to the PC. The resulting set of acoustic signals $p(x, t)$ detected over the entire line-scan were then mapped to a linear grayscale and displayed as a 2D image, as shown in Fig. 5. The image is characterized by an initial tripolar planar wavefront P that arrives at a time corresponding to the perpendicular distance between the sensor detection plane and the transducer. This planar wavefront is then followed by inverted edge waves E originating from the circumference of the transducer which appear as a characteristic X-shaped feature. At the center of the scan the interrogation laser beam lies on the axis of the transducer. The edge wave contributions from each point around the transducer circumference therefore arrive at the same time, producing a signal maximum at the center of the X feature. As the detection point moves off axis, the symmetry is broken and the contributions from different points around the transducer circumference ar-

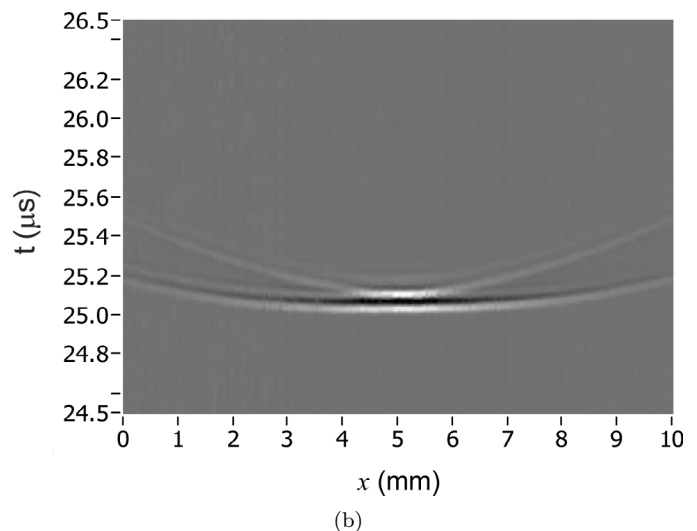
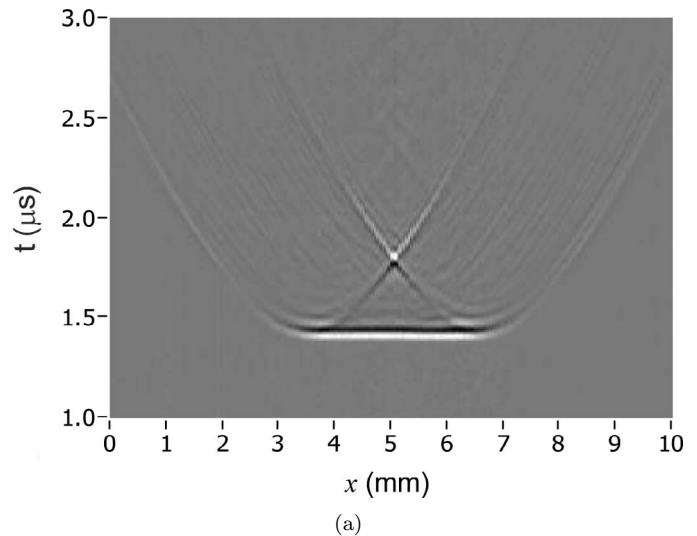


Fig. 6. Line-scans of the output of a pulsed 20-MHz planar PZT transducer of diameter 3.2 mm. Line-scan length $x = 10$ mm, scan step $dx = 50 \mu\text{m}$, spot size $a = 50 \mu\text{m}$, number of signal averages = 128. (a) Near field scan, transducer-sensor distance = 2.1 mm, temporal sampling interval $dt = 2$ ns, image acquisition time = 3.5 minutes. (b) Far field scan, transducer-sensor distance = 37.5 mm, temporal sampling interval $dt = 1$ ns, image acquisition time = 3.5 minutes.

rive at different times, the temporal extremes of which are indicated by the diagonal lines of the X-shaped feature. Similar behavior can be seen in Fig. 6(a). This shows a near field axial line-scan of a higher frequency (20 MHz) transducer (Panametrics V316) of diameter 3.2 mm positioned 2.1 mm from the FP sensor. For comparison, a far field scan of the same transducer but at a distance of 37.5 mm from the sensor is shown in Fig. 6(b), showing the edge wave beginning to merge with the initial plane wavefront.

Finally, the very near field output of a 15-MHz transducer (Panametrics V319) of diameter 12.8 mm positioned 2.7 mm from the FP sensor is shown in Fig. 7. Unlike Figs. 5 and 6, the image is heavily thresholded (35% of maximum amplitude and 6% of the minimum) to reveal

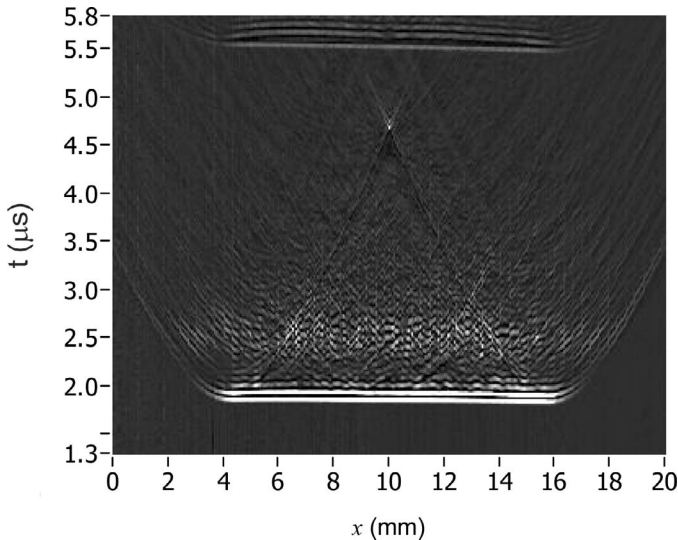


Fig. 7. Line-scan of the output of a pulsed 15-MHz planar PZT transducer of diameter 22 mm positioned 2.7 mm from the FP sensor. Line-scan length $x = 20$ mm, scan step $dx = 50 \mu\text{m}$, spot size $a = 50 \mu\text{m}$, temporal sampling interval $dt = 2$ ns, number of signal averages = 128, image acquisition time = 6.5 minutes.

low amplitude features. The characteristic X-shaped edge wave feature following the arrival of the initial plane wavefront is clearly apparent, as expected. However, there also appears to be significant fine structure within a microsecond or so of the initial plane wavefront, the nature of which is characteristic of a random distribution of discrete sources over the transducer surface—the ability to observe such fine structure illustrating the high spatial-temporal measurement resolution of the system. The plane wavefront at $t \sim 5.5 \mu\text{s}$ corresponds to the time-delayed round trip reflection of the initial plane wavefront between the surface of the sensor and the transducer face.

B. Rapid Mapping of a Focused Transducer

In the examples in the previous section, the acoustic waveforms were downloaded to the PC at each step of the scan. This resulted in relatively long image acquisition times—of the order of several minutes for a line-scan of a few hundred points. To demonstrate the ability to scan at significantly higher speeds, the method referred to in Section II-D, whereby the waveforms for an entire line-scan are captured on a single record by the DSO and transferred to the PC at the end of the scan, was used to map the output of a focused transducer. The latter was a pulsed 5-MHz PZT transducer (Panametrics A307S) of diameter 29 mm and focal length 63.5 mm positioned 48 mm from the FP sensor. The waveforms were captured over a line of length 20 mm in steps of $100 \mu\text{m}$ and are shown in Fig. 8, illustrating the curvature of the off-focus wavefront. In this example, no signal averaging was performed due to the limited record length of the specific DSO used. The acquisition time per scan step was 50 ms, enabling the image shown in Fig. 8 to be obtained in 10 s.

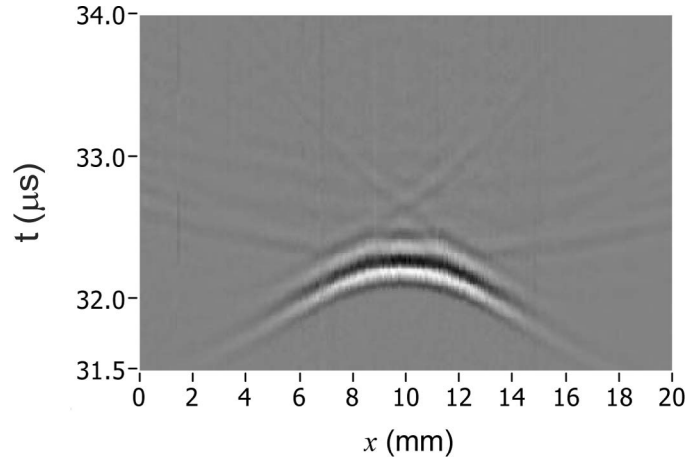


Fig. 8. High-speed mapping of the output of a pulsed 5-MHz focused PZT transducer of diameter 29 mm positioned at distance of 48 mm from the FP sensor. Line-scan length $x = 20$ mm, scan step $dx = 0.1$ mm, spot size $a = 50 \mu\text{m}$, temporal sampling interval $dt = 10$ ns. No signal averaging was used. Image acquisition time = 10 seconds.

V. CONCLUSIONS

A new approach to mapping ultrasound fields based upon optically scanning a wavelength-tuned focused laser beam over a planar FP polymer film sensor has been demonstrated. This system enables broadband ultrasound fields with a frequency content extending to several tens of megahertz to be rapidly mapped with good signal-noise ratios over a 40-mm aperture with $50\text{-}\mu\text{m}$ spatial resolution. There is considerable scope to further optimize the system in terms of the scan parameters and acoustic performance. The current line-scanning instrument could be straightforwardly modified to incorporate an additional galvanometer for two-dimensional mapping and the scan step time, currently limited by the speed of the D-A card used, could be reduced to a few milliseconds enabling the images shown in Section IV-A to be obtained in a fraction of a second. By adjusting both the dimensions of the interrogation beam and the thickness of the polymer film, the bandwidth of the system can readily be extended. In the first instance, the 30-MHz bandwidth of the current system could be increased to 50 MHz by reducing the polymer film thickness to $25 \mu\text{m}$ (currently limited by the tuning range of the VCSEL) and reducing the focused laser spot size and step increment of the scan accordingly to fulfill the spatial Nyquist sampling criterion. Ultimately, the system bandwidth could be extended to several hundred megahertz because the spot size, scan step size, and polymer film thickness can all be reduced to a few microns, although the latter would necessitate the use of a more widely tunable interrogation laser to accommodate the increased FSR of the FPI. Additionally, an increased upper limit of linear detection, for example, for measuring the output of diagnostic medical ultrasound instruments, can be achieved by reducing the thickness of the polymer film or reducing the finesse of the ITF. For example, it was shown previously that an upper limit of linear detection (to within 10%) of

11 MPa is possible using a 25- μm -thick polymer film and a low finesse ITF [17]. For applications where high sensitivity is of overriding importance, it has been shown that, using a laser source with lower phase noise characteristics and higher power than the VCSEL, there is the prospect of improving the NEP by almost two orders of magnitude to 0.1 kPa [16].

In addition to the high degree of flexibility in the scan parameters and acoustic performance, a notable feature of this system is its low cost. This is due to the ability to inexpensively batch fabricate the sensors through the use of vacuum deposition methods and the inexpensive nature of the laser source, the VCSEL. The cost is therefore dominated by the galvanometer, its control electronics, and optical mounting components, making it possible to construct a system for a few thousand dollars.

In summary then, this concept has the potential for use in field mapping applications that require a passive receive array such as photoacoustic and transmission ultrasound imaging and the characterization of fields produced by ultrasound transducers and transducer arrays such as those used in diagnostic and therapeutic medical ultrasound and industrial nondestructive technology.

REFERENCES

- [1] G. Paltauf and H. Schmidt-Kloiber, "Optical method for two dimensional ultrasonic detection," *Appl. Phys. Lett.*, vol. 75, no. 8, pp. 1048–1050, 1999.
- [2] J. D. Hamilton and M. O'Donnell, "High frequency ultrasound imaging with optical arrays," *IEEE Trans. Ultrason., Ferroelect., Freq. Contr.*, vol. 45, no. 1, pp. 216–235, 1998.
- [3] S. A. Carp, A. Guerra, Q. Duque, and V. Vengupalan, "Optoacoustic imaging using interferometric measurement of surface displacement," *Appl. Phys. Lett.*, vol. 85, no. 23, pp. 5772–5774, 2004.
- [4] V. Wilkens and C. Koch, "Optical multilayer detection array for fast ultrasonic field mapping," *Opt. Lett.*, vol. 24, no. 15, pp. 1026–1028, 1999.
- [5] V. Wilkens, "Characterisation of an optical multilayer hydrophone with constant frequency response in the range 1 to 75 MHz," *J. Acoust. Soc. Amer.*, vol. 113, no. 3, pp. 1431–1438, 2003.
- [6] M. Klann and C. Koch, "Measurement of spatial cross sections of ultrasound pressure fields by optical scanning means," *IEEE Trans. Ultrason., Ferroelect., Freq. Contr.*, vol. 52, pp. 1546–1554, 2005.
- [7] J. D. Hamilton, T. Buma, M. Spisar, and M. O'Donnell, "High frequency optoacoustic arrays using etalon detection," *IEEE Trans. Ultrason., Ferroelect., Freq. Contr.*, vol. 47, no. 1, pp. 160–169, 2000.
- [8] P. C. Beard and T. N. Mills, "Extrinsic optical fibre ultrasound sensor using a thin polymer film as a low finesse Fabry-Perot interferometer," *Applied Optics*, vol. 35, no. 4, pp. 663–675, 1996.
- [9] Y. Uno and K. Nakamura, "Pressure sensitivity of a fibre-optic microprobe for high frequency ultrasonic field," *Jpn. J. Appl. Phys.*, vol. 38, pp. 3120–3123, 1999.
- [10] S. Askenazi, R. Witte, and M. O'Donnell, "High frequency ultrasound imaging using a Fabry Perot etalon," *Proc. SPIE*, vol. 5697, pp. 243–250, 2005.
- [11] P. C. Beard and T. N. Mills, "A 2D optical ultrasound array using a polymer film sensing interferometer," in *Proc. IEEE Ultrason. Symp.*, 2000, pp. 1183–1186.
- [12] P. C. Beard, "2D ultrasound receive array using an angle-tuned Fabry Perot polymer film sensor for transducer field characterisation and transmission ultrasound imaging," *IEEE Trans. Ultrason., Ferroelect., Freq. Contr.*, vol. 52, no. 6, pp. 1002–1012, 2005.
- [13] M. Lamont and P. C. Beard, "2D imaging of ultrasound fields using a CCD array to detect the output of a Fabry Perot polymer film sensor," *Electron. Lett.*, vol. 42, no. 3, pp. 187–189, 2006.
- [14] B. T. Cox, E. Z. Zhang, J. G. Laufer, and P. C. Beard, "Fabry Perot polymer film fibre-optic hydrophones and arrays for ultrasound field characterisation," *J. Phys.: Conf. Series*, vol. 1, pp. 32–37, 2004.
- [15] P. C. Beard, F. Perennes, and T. N. Mills, "Transduction mechanisms of the Fabry Perot polymer film sensing concept for wideband ultrasound detection," *IEEE Trans. Ultrason., Ferroelect., Freq. Contr.*, vol. 46, no. 6, pp. 1575–1582, 1999.
- [16] E. Z. Zhang, B. T. Cox, and P. C. Beard, "Ultra high sensitivity, wideband Fabry Perot ultrasound sensors as an alternative to piezoelectric PVDF transducers for biomedical photoacoustic detection," *Proc. SPIE*, vol. 5320, pp. 222–229, 2004.
- [17] P. C. Beard, A. Hurrell, and T. N. Mills, "Characterisation of a polymer film optical fibre hydrophone for the measurement of ultrasound fields for use in the range 1–30 MHz: A comparison with PVDF needle and membrane hydrophones," *IEEE Trans. Ultrason., Ferroelect., Freq. Contr.*, vol. 47, no. 1, pp. 256–264, 2000.